frontiers in Physics

ORIGINAL RESEARCH
published: 17 June 2021
doi: 10.3389/fphy.2021.654845

The Transition From MoS_2 Single-Layer to Bilayer Growth on the Au(111) Surface

Moritz Ewert[1,2,3]*, *Lars Buß*[1,2], *Nicolas Braud*[2,3], *Asish K. Kundu*[4,5], *Polina M. Sheverdyaeva*[4], *Paolo Moras*[4], *Francesca Genuzio*[6], *Tevfik Onur Menteş*[7], *Andrea Locatelli*[7], *Jens Falta*[2,3] and *Jan Ingo Flege*[1,2,3]

[1] Applied Physics and Semiconductor Spectroscopy, Brandenburg University of Technology Cottbus-Senftenberg, Cottbus, Germany, [2] Institute of Solid State Physics, University of Bremen, Bremen, Germany, [3] MAPEX Center for Materials and Processes, University of Bremen, Bremen, Germany, [4] Istituto di Struttura della Materia, Consiglio Nazionale delle Ricerche (ISM-CNR), Trieste, Italy, [5] International Center for Theoretical Physics, Trieste, Italy, [6] Central European Research Infrastructure Consortium (CERIC-ERIC), Trieste, Italy, [7] Elettra-Sincrotrone Trieste S.C.p.A., Trieste, Italy

The transition from single-layer to bilayer growth of molybdenum disulfide on the Au(111) surface is investigated by *in situ* low-energy electron and photoemission microscopy. By mapping the film morphology with nanometer resolution, we show that a MoS_2 bilayer forms at the boundaries of single-layer single-domain MoS_2 islands and next to merging islands whereas bilayer nucleation at the island centers is found to be suppressed, which may be related to the usage of dimethyl disulfide as sulfur precursor in the growth process. This approach, which may open up the possibility of growing continuous films over large areas while delaying bilayer formation, is likely transferable to other transition metal dichalcogenide model systems.

Keywords: LEEM, XPEEM, micro-ARPES, low-energy electron microscopy, molybdenum disulfide, 2D materials, epitaxial growth, Au(111)

OPEN ACCESS

Edited by:
Stiven Forti,
Italian Institute of Technology, Italy

Reviewed by:
Alexei Zakharov,
MAXIV Laboratory, Sweden
Philip Schädlich,
Technische Universität Chemnitz, Germany
Shirley Chiang,
University of California, Davis, United States

***Correspondence:**
Moritz Ewert
mewert@b-tu.de

Specialty section:
This article was submitted to Condensed Matter Physics, a section of the journal Frontiers in Physics

Received: *17 January 2021*
Accepted: *16 April 2021*
Published: *17 June 2021*

Citation:
Ewert M, Buß L, Braud N, Kundu AK, Sheverdyaeva PM, Moras P, Genuzio F, Menteş TO, Locatelli A, Falta J and Flege JI (2021) The Transition From MoS_2 Single-Layer to Bilayer Growth on the Au(111) Surface. Front. Phys. 9:654845. doi: 10.3389/fphy.2021.654845

1. INTRODUCTION

The interest in two-dimensional (2D) materials has been strongly increasing since the seminal discovery of the peculiar electronic properties of graphene in 2004 [1], including Dirac-like dispersion of the electronic bandstructure near the Fermi level [2, 3]. However, in view of applications, as a semi-metal, graphene is not a suitable candidate for electronic devices, such as transistors or optoelectronics [1], because for these applications a sizeable, direct bandgap is necessary. Yet, a promising group of van-der-Waals materials, the transition metal dichalcogenides (TMDs) [4], was identified that can also be thinned down to a 2D material to fill this need. A typical representative of these TMDs is molybdenum disulfide (MoS_2), which may be regarded as a model system to unravel their materials properties. Indeed, a direct bandgap was demonstrated for single-layer MoS_2 in first photoluminescence studies [5, 6]. Subsequently, first proof-of-principle experiments targeting the realization of electronic devices with single-layer MoS_2, such as transistors [7] and photodetectors [8] were reported. Interestingly, although exhibiting an indirect bandgap, also bilayer MoS_2 showed promising electronic applications, e.g., as active channel material in field-effect transistors [9] as well as in novel electronic devices featuring a dynamically tuneable bandgap [10]. Furthermore, even 2D heterostructures combining graphene and MoS_2 could be synthesized, with demonstrated superior performance in optoelectronic devices, such as phototransistors [11], clearly underlining the potential of TMDs for applications.

For the utilization of 2D transition metal dichalcogenides in applications, a scaleable epitaxial growth process is highly desirable. Recent successes in the chemical vapor deposition of MoS_2 layers [12, 13] notwithstanding, one of the key prerequisites to optimizing the growth parameters and conditions is a deeper understanding of the underlying mechanisms governing the formation of single and double layers. Here, we focus on the well-studied model system MoS_2 on Au(111) to gain deeper insights into the epitaxial growth behavior of TMDs and the respective structural transition between single and bilayer coverages. Using a methodology that makes use of several layer-dependent materials properties, e.g., the electron reflectivity for slow electrons and the characteristic electronic bandstructure, we perform a spatially resolved characterization of the synthesized MoS_2 film and are able to map the single-layer and bilayer distribution of MoS_2 with few-nm resolution and reveal key factors determining their formation.

2. MATERIALS AND METHODS

The growth and characterization experiments presented here were performed under ultra-high vacuum (UHV) conditions with a base pressure of 1×10^{-10} torr in an ELMITEC low-energy electron microscopy (LEEM) III at the University of Bremen, Germany, and an ELMITEC SPE-LEEM installed at the Nanospectroscopy beamline at the Elettra Sincrotrone laboratory, Trieste, Italy. Further measurements were performed *ex situ* at the VUV-Photoemission beamline, also at Elettra.

The *in situ* characterization of the MoS_2 growth relies on the real-space and reciprocal-space imaging capabilities of the LEEM system. In real-space imaging mode a spatial resolution of $<$10 nm is achieved under optimized conditions. Generally, the LEEM operates as a full-field microscope, enabling efficient monitoring of the sample surface at video-frame rates. As the LEEM is set up to image the surface employing a range of electron kinetic energies, the local energy-dependent electron reflectivity, the so-called I(V) curve, can be determined from a sequence of real-space images, facilitating the investigation of the local structure. Here, we extract the local I(V) curve in a typical energy range from 2 to 40 eV, in which the influence of the material specific bandstructure, i.e., the dispersion of the unoccupied electronic states of the sample, is most prominent. This reflectivity curve can be calculated using *ab initio* scattering theory; in practice, it can be used as a fingerprint to identify the related material locally [14].

As the LEEM is a diffraction-based microscope, switching between real-space and reciprocal-space imaging is readily possible by adjusting the excitations of the electromagnetic lenses in the imaging column of the instrument. This allows for low-energy electron diffraction (LEED) measurements of the illuminated area on the sample surface, which can be spatially limited down to 250 nm (in the Bremen LEEM) or 500 nm (in the SPE-LEEM at Elettra) in diameter using suitable illumination apertures. By positioning an aperture in the backfocal plane of the objective lens, a single diffracted beam can be selected for real-space imaging. Employing the specular (00) beam allows for bright-field imaging, while any other diffracted beam enables a so-called dark-field measurement. Dark-field imaging reveals the sample area contributing to the selected beam, which in our present case allows to differentiate between the two existing mirror domains of MoS_2 on Au(111) [15, 16].

The spectroscopic photoemission and low-energy electron microscope (SPE-LEEM) at the Nanospectroscopy beamline of the Elettra synchrotron laboratory uses monochromatized soft x-rays in the range of 25–1,000 eV with a hemispherical bandpass energy filter, which is normally operated at a pass energy of 908 eV and an energy resolution of down to 0.2 eV in suitable conditions [17]. The monochromatized synchrotron radiation illuminates the sample and excites photoelectrons of the sample, thereby making it possible to access the bandstructure of the occupied states *via* local angle-resolved photo electron spectroscopy (ARPES) measurements. In accordance with the literature, in the present work a photon energy of 49 eV has been selected to maximize the intensity of the top-most valence band of MoS_2 [18]. Furthermore, in our microspot-ARPES experiments, the contributing surface region of the sample has been limited with a selected-area aperture down to about 2 μm in diameter. Further information on (SPE-)LEEM methodology can be found elsewhere [19–21].

In addition to selected-area ARPES, we also present high-resolution ARPES data, which were recorded *ex situ* at the VUV beamline [22] at Elettra at 49 eV photon energy at about 50 K, using a Scienta R4000 electron energy analyzer with an angular acceptance angle of 30° and an energy resolution of 20 meV.

In the experiments, a Au(111) single crystal was employed as substrate, which was cleaned by several cycles consisting of first Ar^+ sputtering at 0.5 kV for 1 h followed by thermal annealing at 700°C for 30 min. In a final step before starting the growth procedure, the sample was heated to 950°C and annealed for 5 min to ensure a well-defined herringbone reconstruction, which is typical for the clean, well-ordered Au(111) surface [23].

The MoS_2 growth was performed at a sample temperature of 720°C by dosing dimethyldisulfide (DMDS, purity $\geq$99.0%), a vapor sulfur source suitable for MoS_2 growth [24], via chamber backfilling at 1×10^{-6} torr. To ensure full sulfidization during the MoS_2 growth process the sample was exposed to DMDS for 10 min before evaporating the Mo from a Mo metal rod (purity $\geq$99.95%) using e-beam bombardment. After the deposition, a growth rate of 0.2 ML/h was determined from the overall coverage of MoS_2 islands on the Au(111) surface as revealed by large-scale LEEM investigations in relation to the total evaporation time. A detailed report on the growth methodology is published elsewhere [15].

3. RESULTS AND DISCUSSION

In our approach to study the model system MoS_2 on Au(111) we have applied a previously established growth method [15] to achieve MoS_2 islands of mostly one of the two rotational domains close to full coverage. The whole growth process was monitored *in situ* by LEEM. A time-lapse sequence is shown in **Figure 1**,

in which **Figures 1A–C** capture the growth process at three intermediate stages and (D) shows the final state of the sample surface. **Figures 1A–C** focuses on the same region of the sample at a coverage of (A) 0.1 ML, (B) 0.4 ML, and (C) 0.7 ML. These LEEM images are taken with a kinetic electron energy of 16 eV, at which the Au sample surface appears bright and the MoS_2 islands dark. Additionally, one can spot fine dark lines representing the Au step edges and step bunches as well as tiny dark dots that belong to pinning centers of the Au(111) surface. Moreover, one can readily discern the triangular shape of the growing MoS_2 islands during the growth process. The final coverage is shown in **Figure 1D** for 0.9 ML at a kinetic electron energy of 5.2 eV. At this energy the contrast is inverted; the MoS_2 islands appear bright and the Au(111) surface appears dark. Although the MoS_2 islands seem to have expanded with no clear shape at first glance, the *in situ* observations document an island expansion process that proceeds until morphological boundaries limit the island growth, and secondary nucleation of single-layer islands occurs between existing islands once the expansion is limited [15]. The evaporation of Mo and the supply of DMDS was stopped when no further island expansion was observed.

A micro-LEED measurement of a single MoS_2 island provides a clear diffraction pattern with the 3-fold symmetry and moiré spots around specular and integer spots as shown in **Figure 2A**. This indicates a high level of crystalline ordering and structural quality within the MoS_2 island. The 3-fold symmetric pattern is typical for single-domain MoS_2 on Au(111) [25]. Furthermore, this 3-fold symmetry allows mirror domains of single-layer MoS_2 on Au(111) to be identified in dark-field (DF) LEEM by their integer beam intensity [15], similarly to the case of WS_2 on Au(111) [16]. Accordingly, their spatial distribution can be visualized by DF-LEEM performed at distinct electron energies (here, 31 and 41 eV) as demonstrated in **Figures 2C,D**. The extracted (10) beam profiles (see **Figure 2B**) belong to the two mirror domains (cf. **Figures 2C,D** red and black arrows). Using this information, we could determine a distribution of about 90:10 between the two domains of MoS_2 on Au(111). A high-resolution investigation of the electronic bandstructure of the 0.9 ML sample presented in **Figure 1D** was performed at the VUV-Photoemission beamline at Elettra. In the measurement, the sampling area amounted to about 0.3 mm in diameter. The valence band dispersion along the $\bar{\Gamma} - \bar{K}$ direction of the MoS_2 surface Brillouin zone is displayed in **Figure 3A**. The presented ARPES data not only shows the electronic bandstructure of the MoS_2 layer, but is also affected by the underlying gold substrate as already discussed by Miwa et al. [26]. Furthermore, comparing our ARPES data of MoS_2 on Au(111) to exfoliated MoS_2 on SiO_2 we do not find any evidence for a valence band compression, indicative of negligible interaction with the substrate [27]. More specifically, two band maxima are found, a higher one at the $\bar{\Gamma}$ point and a lower one at the $\bar{K}$ point, exhibiting a relative energy difference of 0.35 eV. Additionally, at the $\bar{K}$ point a spin splitting of 0.14 eV as well as the gold surface states are observed, in good agreement with previous studies [26]. Taken together, these findings represent the typical tell-tale signs of the electronic bandstructure of 2H-stacked MoS_2 bilayers [28], which raises the question where these bilayer regions may be found on the sample surface.

Since the employed growth method provides relatively large MoS_2 islands of few micrometer size, these may be suitable for assessing the electronic structure of the single-layer and bilayer MoS_2 regions separately in selected-area ARPES measurements, possibly also allowing insights into the yet unknown spatial distribution of the bilayer areas. The respective data taken from two distinct sample regions, each about 2 μm in diameter, are presented in **Figures 3B–E**.

From both regions, local 2D photoelectron angular distribution patterns were acquired at several electron kinetic energies near the Fermi level to scan the three-dimensional (3D) energy-momentum electronic bandstructure. As one can see from the selected-area ARPES data reproduced in **Figures 3B,C**, both regions exhibit a 3-fold symmetric intensity distribution of the first order $\bar{\Gamma}$ points. However, this 3-fold distribution is rotated by 60° between the two regions and accordingly reflects the different orientation of the unit cells. Therefore, these sample regions represent the two mirror domains. From the 3D datasets we derived the band dispersion along the $-\bar{K} - \bar{\Gamma} - \bar{K}$ direction. Both domains exhibit single- and bilayer features (not shown). The latter are found to be more strongly pronounced in a local measurement of a third area that included a high density of island boundaries as shown in **Figure 3D**. In this case, the bandstructure exhibits a band maximum at $\bar{\Gamma}$ point that is 0.35 eV higher than the maximum at the $\bar{K}$ point. This is characteristic for bilayer MoS_2 and in very good agreement with a previous study by Grønborg et al. [28]. Unfortunately, a single island that was large enough for the sampling area not to include any island boundaries was not found on this sample.

To prove the single-layer character of the islands at an intermediate stage of the growth process, a reference sample was produced following an identical preparation procedure as before. Yet, this time the growth was stopped when the MoS_2 islands had reached 1.5–2 μm in size and were perfectly suited for acquiring a single-island single-domain bandstructure. **Figure 3E** displays the respective dispersion along the $-\bar{K} - \bar{\Gamma} - \bar{K}$ direction that has been recorded at the growth temperature, which therefore features substantial thermal broadening. Nevertheless, the maximum at the $\bar{K}$ point is about 0.3 eV higher than the local maximum at $\bar{\Gamma}$ when comparing the intensity centers, in acceptable agreement with previous findings for single-layer MoS_2. This result clearly demonstrates that huge single-domain single-layer MoS_2 islands even with a high local coverage can be achieved, hinting toward a growth scenario in which the limitation in island expansion leads to bilayer formation at the island boundaries. This hypothesis can be investigated in the same instrument by performing x-ray photoemission electron microscopy (XPEEM), i.e., by spectroscopic imaging of the spatial distribution of the elements.

X-ray photoemission electron microscopy images highlighting the elemental gold and sulfur distributions of the same sample area are represented in **Figures 4A,B**, respectively. In both images, three major intensity levels (dark, gray, and bright) are readily discernible, each corresponding to a low, intermediate, and high local elemental concentration.

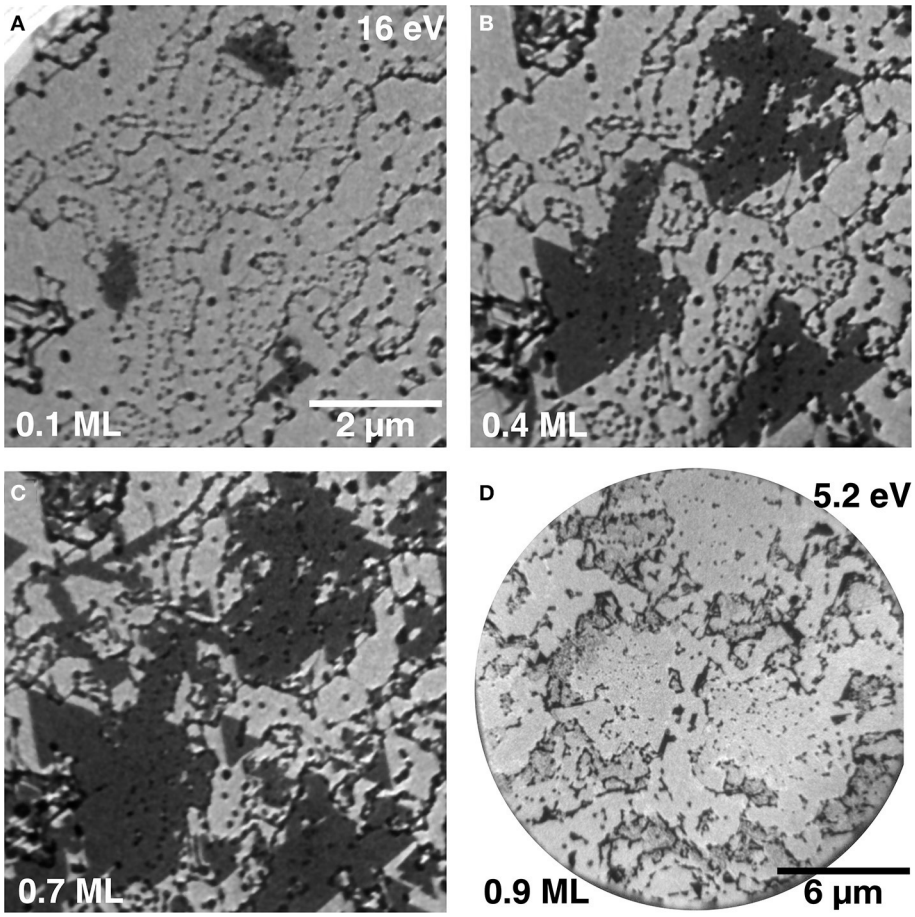

FIGURE 1 | Low-energy electron microscopy (LEEM) time-lapse sequence of the MoS_2 growth process recorded at 16 eV kinetic energy with the Au surface appearing bright and the MoS_2 islands appearing dark for coverages of **(A)** 0.1 ML, **(B)** 0.4 ML, and **(C)** 0.7 ML. An overview LEEM image of the final coverage of 0.9 ML taken at 5.2 eV is shown in **(D)**, where the MoS_2 appears bright and the Au substrate appears dark.

In **Figure 4B**, exemplary regions of intermediate and high sulfur concentrations are marked by red and green arrows, respectively.

Comparing **Figures 4A,B** reveals that the same structural features are visible in both XPEEM images; however, the contrast is found to be reversed. This is readily explained by the attenuation of the Au4f photoelectron intensity caused by the presence of MoS_2 due to inelastic scattering. As the loss of primary photoelectron intensity is proportional to the local amount of MoS_2 on-top, the distinct gray levels are thus representing different local film thicknesses. Accordingly, the highest Au4f intensity corresponds to still uncovered sample areas, the next-highest to 1 ML MoS_2 islands (gray contrast), and the lowest intensity to 2 ML patches. Likewise, the patches with the highest Au intensity have the least, albeit non-vanishing S2p intensity, consistent with sulfur atoms chemisorbed to the gold substrate in the MoS_2-free regions. The gray areas in the Au4f XPEEM image comprise the largest fraction of the surface and correspond to the intermediate S intensity, marking the single-layer MoS_2 islands. Consequently, the thin lines and patches that show up dark (bright) in the Au4f (S2p) image are consistently interpreted as bilayer MoS_2 regions, which appear to decorate the single-layer island boundaries. Hence, the XPEEM data strongly suggest the coexistence of single-layer and bilayer MoS_2 islands on a length scale that prevents a clear separation in selected-area ARPES. This interpretation is validated using IV-LEEM, a technique that is able to quantify the local film thickness in terms of S-Mo-S monolayers.

The conditions leading to bilayer growth can further be elucidated when the local MoS_2 morphology is probed at a higher spatial resolution. The inset in **Figure 5** shows the nearly closed monolayer of MoS_2 on Au(111) as observed in the LEEM. The presented measurement of the electron reflectivity by I(V)-LEEM of the differently covered regions reveal the corresponding reflectivity curves that can be used as identifying fingerprints for each region and to quantitatively determine the local number of MoS_2 layers, in analogy to graphene [30]. Specifically, in the energy range from about 3 to about 9 eV, the curve of the single-layer MoS_2 shows one characteristic dip at 7.6 eV (cf. green solid line) whereas the bilayer exhibits two characteristic dips

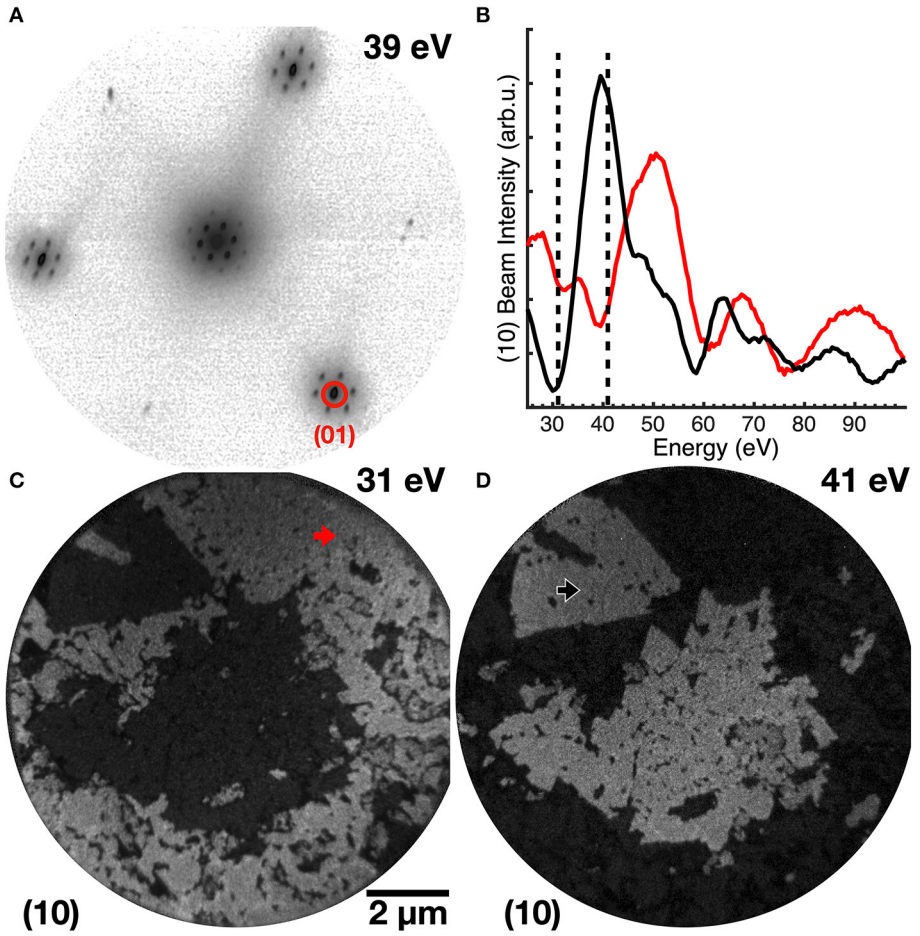

FIGURE 2 | Dark-field low-energy electron microscopy (DF-LEEM) measurement using the (10) beam of the MoS_2 LEED pattern, as seen in **(A)** at 39 eV. The integer beam intensity of each domain is shown in **(B)**. At the two indicated energies only one of the domains significantly contributes to the beam intensity and thus appears bright: **(C)** majority domain (red line and arrow) and **(D)** minority domain (dark line and arrow). No traces of the BL-MoS_2 (cf. **Figure 5**) are visible in the dark appearing domain.

at 5.2 and 7.8 eV (cf. red solid line). These reflectivity curves are in good agreement with measurements of exfoliated MoS_2 on hBN by de Jong et al. [29] and in excellent agreement with the calculated reflectivity profiles from *ab initio* scattering theory (cf. dashed lines in **Figure 5**) as reported by the same authors, clearly justifying the assigned numbers of local MoS_2 layers. However, we note that these two transmission resonances in the I(V) curve are of entirely different origin: Since the dip at 7.6 eV is perfectly reproduced by the *ab initio* calculation assuming a completely free-standing single layer of MoS_2 without a substrate, this particular resonance is most probably intrinsically related to the internal three-layer structure of the S-Mo-S trilayer. This is different from the situation in free-standing single-layer graphene, where no transmission resonance is found [31]. Yet, adding a second MoS_2 layer gives rise to the evolution of a Fabry-Pérot-like interference minimum, which accordingly is found at 5.2 eV.

In total, on the sample surface, three types of regions are found, each identified by their unique reflectivity curves. At the displayed energy of 7.6 eV (cf. inset of **Figure 5**), the MoS_2-free Au sample surface appears dark, the micron-sized MoS_2 single-layer single-domain regions gray (cf. green arrow) and the bilayer regions bright (cf. red arrow). Interestingly, this last region is indeed located at the boundaries of the single-layer islands, in excellent agreement with the XPEEM results and also in accordance with our structural ARPES interpretation.

It may, perhaps, be astonishing that we did not observe any indication for bilayer growth in DF-LEEM (**Figure 2**). Similar to the differences found in the (10) and (01) beam intensities between the mirror domains in DF-LEEM, the 2H-stacked MoS_2 bilayer should also exhibit a decisive difference in the integer beam reflectivity compared to the underlying single-layer. This intensity difference can qualitatively be understood by realizing that in the 2H-stacked bilayer the top layer unit mesh is rotated by 60° with respect to the first layer unit mesh, inducing differences in the local structure factor leading to changes in $q_{\|}$-dependent I(V) measurements, with the bottom layer unit mesh being identical to the one of the whole majority-domain

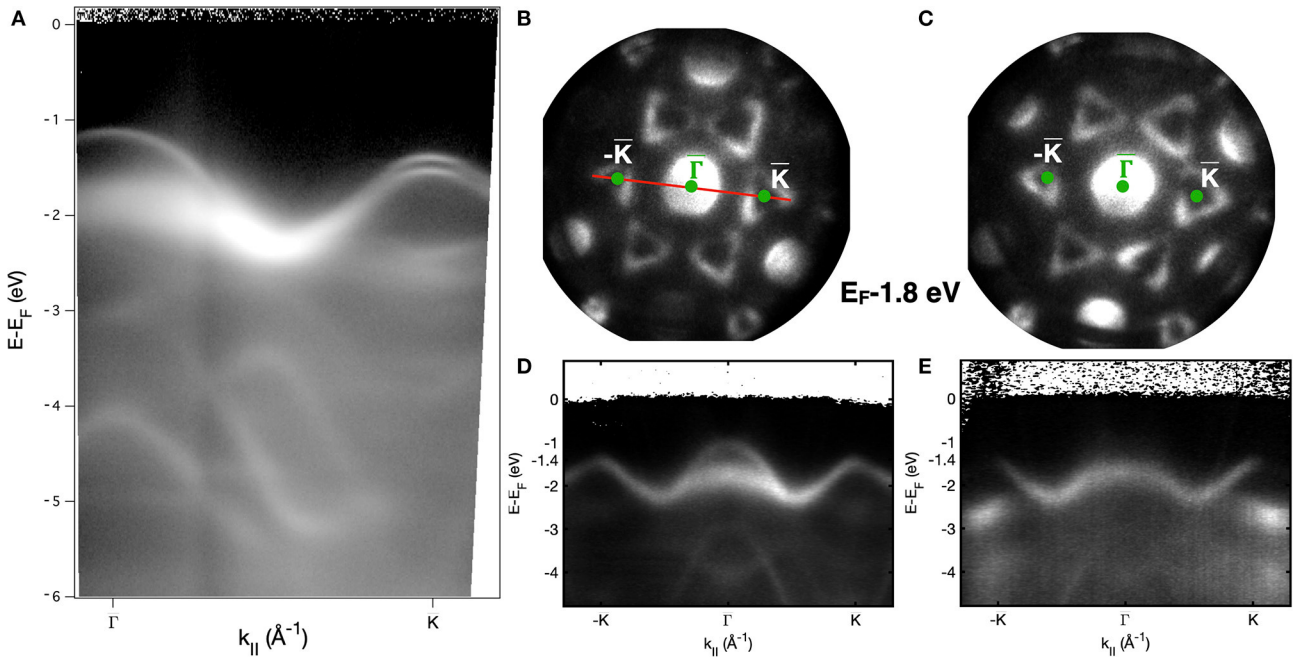

FIGURE 3 | (A) A more detailed measurement of bilayer MoS_2 along the $\bar{\Gamma} - \bar{K}$ direction shows the band splitting of 0.14 eV at the $\bar{K}$ point; the gap between the band maxima at $\bar{\Gamma}$ and $\bar{K}$ is 0.35 eV, which is not observed for single-layer MoS_2. **(B,C)** Two-dimensional photoelectron angular distribution patterns of the two MoS_2 mirror domains at 1.8 eV below the Fermi level from selected-area ARPES measurements. Both the minority domain (see **B**) and the majority domain (see **C**) exhibit a 3-fold symmetry of the first order $\bar{\Gamma}$ points in a mirror configuration. The ARPES data along the $-\bar{K} - \bar{\Gamma} - \bar{K}$ direction (exemplarily indicated by the red line in **B**) exhibits the typical bandstructures for **(D)** bilayer MoS_2 (recorded at RT), with an additional band at the $\bar{\Gamma}$ point for the bilayer, and **(E)** for single-layer MoS_2 (recorded at 720°C).

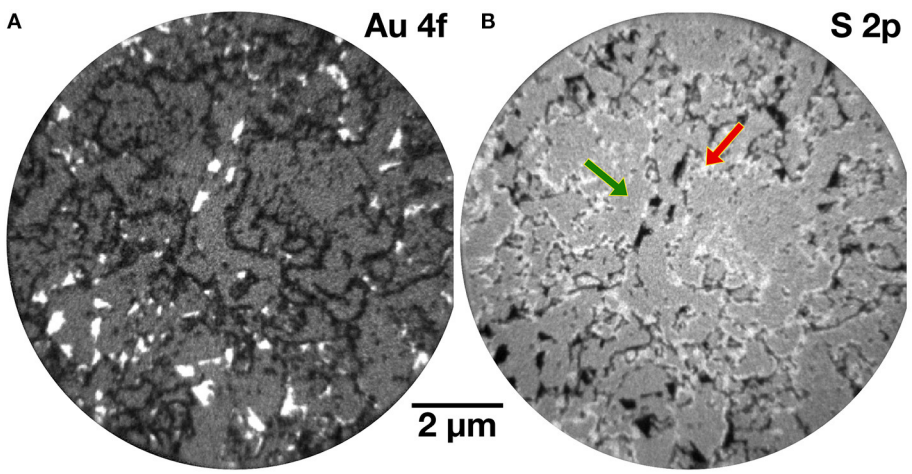

FIGURE 4 | X-ray photoemission electron microscopy (XPEEM) data recorded using $Au4f_{7/2}$ **(A)** and $S2p_{3/2}$ **(B)** core-level photoelectrons (photon energy $h\nu \approx 250$ eV). In **(B)**, an exemplary region of intermediate (high) sulfur concentration is marked by a green (red) arrow, respectively. For comparison, the same regions are also marked in the inset of **Figure 5**.

single-layer MoS_2 island. In fact, a similar observation for single-layer and bilayer MoS_2 has been reported by de Jong et al. [29] for exfoliated MoS_2 deposited on hexagonal boron nitride. As the key differences in the (10) and (01) I(V) curves in this energy range from 25 to 90 eV (in which the surface sensitivity is the highest) mostly originate from the rotation of the MoS_2 unit cell, in DF-LEEM, this reasoning would also lead to a very similar appearance of a single-layer domain and a mirror-symmetrical 2H-stacked bilayer domain. The fact that we did not observe any contrast between the single-layer and bilayer regions (cf. **Figures 2C,D**) may thus indicate non-ideal imaging conditions or insufficient statistics in the DF-LEEM measurement. Yet

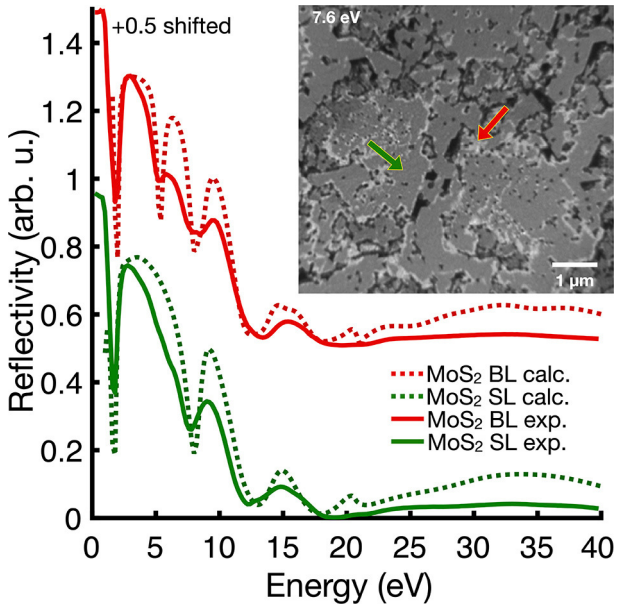

FIGURE 5 | I(V)-LEEM dataset of two MoS_2 regions in the corresponding LEEM image (see inset). The gray region (green arrow and line) is identified as single-layer MoS_2 and the white region (red arrow and line) as bilayer MoS_2 (shifted by +0.5, for clarity). The calculated reflectivity curves of single and bilayer MoS_2 as reported by de Jong et al. [29] are plotted in dashed lines and prove the assignment.

another possible explanation would be a scenario in which the bilayer forms underneath the single-layer island as this would lead to a non-rotated diffraction pattern for the bilayer area and thereby negligible DF-LEEM contrast within a single MoS_2 domain.

The differentiation between single- and bilayer areas owing to the high spatial resolution offered by I(V)-LEEM allows conclusions to be drawn with respect to the bilayer nucleation site as well as some of the key factors influencing bilayer growth at these conditions. From **Figure 5**, it can clearly be concluded that the bilayer has grown only in areas of merging single-layer islands or at island boundaries themselves, but not in the island centers. Additional I(V)-LEEM observations on a step-rich Au(111) surface (not shown) further point toward bilayer formation at the island boundaries of micrometer-sized single-domain MoS_2 islands already at a lower coverage (i.e. 0.3 ML), when the island expansion process is limited by Au step bunches.

We compare our results for this model system of MoS_2 on Au(111) to an epitaxial growth study reported by Grønborg et al., who were also able to identify bilayer islands [28]. For clarity, we, here, repeat the most important findings: Employing a growth method based on cycled nanocluster growth at a temperature of 850 K with H_2S as sulfur precursor, they report a merging of the single-layer islands at about 0.6 ML leading to domain boundaries between nanoclusters within an island. The bilayer itself, which forms at coverages close to a monolayer, has been identified as 2H-stacked MoS_2, and the respective island shape is described as not as clear as observed for the single-layer MoS_2 at similar coverages. Furthermore, the irregular contours have been linked to the growth of the second layer owing to the weak van-der-Waals interaction between the MoS_2 layers, which is assumed to cause the occurrence of many rotational domains and which, accordingly, might explain the unclear shape. Yet, a tendency of bilayer nucleation at island or domain boundaries has not been reported.

Although the experimental conditions of Grønborg et al. [28] differ from ours, MoS_2 bilayers are found in both studies. But, whereas Grønborg et al. identified the overall coverage as the key factor, we find that it is indeed the local coverage on the micrometer scale that tips the balance toward bilayer nucleation. Moreover, another factor is the limitation of the single-layer island expansion that seems to force the bilayer formation upon continued growth. This limitation may be imposed by the proximity of other MoS_2 islands or the substrate morphology itself. Apart from other potential kinetic factors (e.g., related to the deposition rate), only under these circumstances is the MoS_2 likely to grow the second layer rather than expanding the first. Moreover, the specific choice of sulfur agent (e.g., H_2S or DMDS) does also impact the bilayer formation process: Whereas the H_2S-supported growth has been reported to form bilayer clusters in the island centers [28], this is not the case when DMDS is used even though both agents were found to form MoS_2 at similar quality [24]. Our finding that DMDS-supported MoS_2 growth only forms bilayer close to the island boundaries suggests that in the present case the bilayer growth is limited by the DMDS dissociation occurring on the Au(111) surface only. However, when using H_2S as precursor, S is continuously provided since the H_2S may also dissociate on the MoS_2 islands, thus facilitating local bilayer growth. Summarizing this discussion, our results establish two key factors that are responsible for bilayer formation, i.e., (i) a limitation in the island expansion imposed by near-by islands or surface obstacles (e.g., step bunches) and (ii) the local availability of sulfur following dissociation of the S-containing precursor molecules.

4. CONCLUSIONS

The epitaxial growth of MoS_2 by reactive molecular beam epitaxy was studied on the Au(111) single crystal surface using *in situ* and *ex situ* experimental methods including low-energy electron and spectroscopic photoemission microscopy.

The coexistence of single- and bilayer MoS_2 was successfully identified by micro-ARPES and XPEEM as well as I(V)-LEEM measurements, the last being able to provide nanometer-scale information on the film morphology and thickness. We located the formation of MoS_2 bilayer patches at the boundaries of MoS_2 single-layer islands whereas the island center remain bilayer-free for our preparation conditions, specifically using DMDS as sulfur precursor. Together with our *in situ* LEEM observations during growth, these findings suggest that the

key factors for bilayer formation are related to the substrate and film morphology during growth that may limit the MoS_2 island expansion, e.g., by Au step bunches or merging with adjacent MoS_2 islands. Our observation that bilayer nucleation does not occur at the island centers is likely related to the usage of DMDS instead of H_2S as sulfur source, for which bilayer patches have previously been found far away from the single-layer island edges. This interpretation may be clarified in future detailed study of DMDS chemistry on MoS_2 single-layer islands including mapping of the sulfur distribution. These issues notwithstanding, we conclude that using a sulfur agent which does only supply sulfur to the substrate may be key to pure single-layer MoS_2 on the Au(111) surface. This key ingredient of our growth recipe, as well as these considerations, may well be transferable to the growth of related transition-metal dichalcogenides (e.g., WS_2) on Au(111) or other transition metal surfaces.

DATA AVAILABILITY STATEMENT

The raw data supporting the conclusions of this article will be made available by the authors, without undue reservation.

AUTHOR CONTRIBUTIONS

ME, JF, and JIF designed the study. ME performed the experiments as well as processed the experimental data, performed the initial analysis, and designed the figures. LB helped to perform and assisted in the LEEM, VUV-ARPES, and SPE-LEEM experiments. PS, AK, and PM supervised and assisted with the VUV-ARPES measurements. NB and JIF participated in the VUV-ARPES measurements. TM, FG, and AL supervised and assisted with the SPE-LEEM measurements. JIF and JF supervised the project. ME and JIF wrote the manuscript. All authors discussed the results and interpretation and contributed to the final manuscript.

FUNDING

We gratefully acknowledge support by the Central Research Fund of the University of Bremen. The research leading to this result has been supported by the project CALIPSOplus under Grant Agreement 730872 from the EU Framework Programme for Research and Innovation HORIZON 2020. AK acknowledges the receipt of a fellowship from the ICTP-TRIL Programme, Trieste, Italy.

REFERENCES

1. Novoselov KS, Geim AK, Morozov SV, Jiang D, Zhang Y, Dubonos SV, et al. Electric field in atomically thin carbon films. *Science*. (2004) 306:666–9. doi: 10.1126/science.1102896
2. Novoselov KS, Geim AK, Morozov SV, Jiang D, Katsnelson MI, Grigorieva IV, et al. Two-dimensional gas of massless Dirac fermions in graphene. *Nature*. (2005) 438:197–200. doi: 10.1038/nature04233
3. Castro Neto AH. Graphene: phonons behaving badly. *Nat Mater*. (2007) 6:176–7. doi: 10.1038/nmat1851
4. Novoselov KS, Jiang D, Schedin F, Booth TJ, Khotkevich VV, Morozov SV, et al. Two-dimensional atomic crystals. *Proc Natl Acad Sci USA*. (2005) 102:10451–3. doi: 10.1073/pnas.0502848102
5. Mak KF, Lee C, Hone J, Shan J, Heinz TF. Atomically thin MoS_2: a new direct-gap semiconductor. *Phys Rev Lett*. (2010) 105:136805. doi: 10.1103/PhysRevLett.105.136805
6. Splendiani A, Sun L, Zhang Y, Li T, Kim J, Chim CY, et al. Emerging photoluminescence in monolayer MoS_2. *Nano Lett*. (2010) 10:1271–5. doi: 10.1021/nl903868w
7. Radisavljevic B, Radenovic A, Brivio J, Giacometti V, Kis A. Single-layer MoS_2 transistors. *Nat Nanotechnol*. (2011) 6:147–50. doi: 10.1038/nnano.2010.279
8. Lopez-Sanchez O, Lembke D, Kayci M, Radenovic A, Kis A. Ultrasensitive photodetectors based on monolayer MoS_2. *Nat Nanotechnol*. (2013) 8:497–501. doi: 10.1038/nnano.2013.100
9. Wang H, Yu L, Lee YH, Shi Y, Hsu A, Chin ML, et al. Integrated circuits based on bilayer MoS_2 transistors. *Nano Lett*. (2012) 12:4674–80. doi: 10.1021/nl302015v
10. Chu T, Ilatikhameneh H, Klimeck G, Rahman R, Chen Z. Electrically tunable bandgaps in bilayer MoS_2. *Nano Lett*. (2015) 15:8000–7. doi: 10.1021/acs.nanolett.5b03218
11. Chen C, Feng Z, Feng Y, Yue Y, Qin C, Zhang D, et al. Large-scale synthesis of a uniform film of bilayer MoS_2 on graphene for 2D heterostructure phototransistors. *ACS Appl Mater Interfaces*. (2016) 8:19004–11. doi: 10.1021/acsami.6b00751
12. Dumcenco D, Ovchinnikov D, Marinov K, Lazić P, Gibertini M, Marzari N, et al. Large-area epitaxial monolayer MoS_2. *ACS Nano*. (2015) 9:4611–20. doi: 10.1021/acsnano.5b01281
13. Yu H, Liao M, Zhao W, Liu G, Zhou XJ, Wei Z, et al. Wafer-scale growth and transfer of highly-oriented monolayer MoS_2 continuous films. *ACS Nano*. (2017) 11:12001–7. doi: 10.1021/acsnano.7b03819
14. Flege JI, Krasovskii EE. Intensity-voltage low-energy electron microscopy for functional materials characterization. *Phys Status Solidi Rapid Res Lett*. (2014) 8:463–77. doi: 10.1002/pssr.201409102
15. Ewert M, Buß L, Lauritsen JV, Falta J, Flege JI. The mechanism for single-domain single-layer MoS_2 growth on Au(111). *arXiv [Preprint]*. (2021). Available online at: https://arxiv.org/abs/2105.03294
16. Bignardi L, Lizzit D, Bana H, Travaglia E, Lacovig P, Sanders CE, et al. Growth and structure of singly oriented single-layer tungsten disulfide on Au(111). *Phys Rev Mater*. (2019) 3:014003. doi: 10.1103/PhysRevMaterials.3.014003
17. Menteş TO, Zamborlini G, Sala A, Locatelli A. Cathode lens spectromicroscopy: methodology and applications. *Beilstein J Nanotechnol*. (2014) 5:1873–86. doi: 10.3762/bjnano.5.198
18. Bruix A, Miwa JA, Hauptmann N, Wegner D, Ulstrup S, Grønborg SS, et al. Single-layer MoS_2 on Au: band gap renormalization and substrate interaction. *Phys Rev B*. (2016) 93:165422. doi: 10.1103/PhysRevB.93.165422
19. Bauer E. *Surface Microscopy With Low Energy Electrons*. vol. 9781493909. New York, NY: Springer New York (2014). doi: 10.1007/978-1-4939-0935-3
20. Flege JI, Tang WX, Altman MS. Low-energy electron microscopy. In: Kaufmann EN, editor. *Characterization of Materials*. Hoboken, NJ, USA: John Wiley & Sons, Inc. (2012). p. 1808–27. doi: 10.1002/0471266965.com157
21. Locatelli A, Bauer E. Recent advances in chemical and magnetic imaging of surfaces and interfaces by XPEEM. *J Phys Condens Matter*. (2008) 20:093002. doi: 10.1088/0953-8984/20/9/093002
22. Elettra-Sincrotrone Trieste SCpA. *VUV Photoemission Beamline*. (2020). Available online at: https://www.elettra.eu/elettra-beamlines/vuv.html
23. Barth JVV, Brune H, Ertl G, Behm RJ. Scanning tunneling microscopy observations on the reconstructed Au(111) surface: atomic structure, lon-range superstructure, rotational domains, and surface defects. *Phys Rev B*. (1990) 42:9307–18. doi: 10.1103/PhysRevB.42.9307
24. Tuxen A, Gøbel H, Hinnemann B, Li Z, Knudsen KG, Topsøe H, et al. An atomic-scale investigation of carbon in MoS_2 hydrotreating catalysts sulfided by organosulfur compounds. *J Catal*. (2011) 281:345–51. doi: 10.1016/j.jcat.2011.05.018

25. Bana H, Travaglia E, Bignardi L, Lacovig P, Sanders CE, Dendzik M, et al. Epitaxial growth of single-orientation high-quality MoS_2 monolayers. *2D Mater*. (2018) 5:35012. doi: 10.1088/2053-1583/aabb74
26. Miwa JA, Ulstrup S, Sørensen SG, Dendzik M, Čabo AG, Bianchi M, et al. Electronic structure of epitaxial single-layer MoS_2. *Phys Rev Lett*. (2015) 114:046802. doi: 10.1103/PhysRevLett.114.046802
27. Jin W, Yeh PC, Zaki N, Zhang D, Sadowski JT, Al-Mahboob A, et al. Direct measurement of the thickness-dependent electronic band structure of MoS_2 using angle-resolved photoemission spectroscopy. *Phys Rev Lett*. (2013) 111:106801. doi: 10.1103/PhysRevLett.111.106801
28. Grønborg SS, Ulstrup S, Bianchi M, Dendzik M, Sanders CE, Lauritsen JV, et al. Synthesis of epitaxial single-layer MoS_2 on Au(111). *Langmuir*. (2015) 31:9700–6. doi: 10.1021/acs.langmuir.5b02533
29. de Jong TA, Jobst J, Yoo H, Krasovskii EE, Kim P, van der Molen SJ. Measuring the local twist angle and layer arrangement in Van der Waals heterostructures. *Phys Status Solidi B*. (2018) 255:1800191. doi: 10.1002/pssb.201800191
30. Hibino H, Kageshima H, Maeda F, Nagase M, Kobayashi Y, Yamaguchi H. Microscopic thickness determination of thin graphite films formed on SiC from quantized oscillation in reflectivity of low-energy electrons. *Phys Rev B*. (2008) 77:075413. doi: 10.1103/PhysRevB.77.075413
31. Nazarov VU, Krasovskii EE, Silkin VM. Scattering resonances in two-dimensional crystals with application to graphene. *Phys Rev B*. (2013) 87:041405. doi: 10.1103/PhysRevB.87.041405

Conflict of Interest: The authors declare that the research was conducted in the absence of any commercial or financial relationships that could be construed as a potential conflict of interest.

The handling editor declared a past co-authorship with one of the authors JF.